LM-01K062
June 15, 2001

Infrared Frequency Selective Surfaces Fabricated using Optical Lithography and Phase-Shift Masks

S.J. Spector, D.K. Astolfi, S.P. Doran, T.M. Lyszczarz, J.E. Raynolds

Infrared Frequency Selective Surfaces Fabricated using Optical Lithography and Phase-Shift Masks.

S. J. Spector*, D.K. Astolfi, S. P. Doran and T. M. Lyszczarz
Lincoln Laboratory Massachusetts Institute of Technology, Lexington, MA 02420-9108

J. E. Raynolds
Lockheed Martin, Schenectady, NY 12301-1072

Abstract

A frequency selective surface (FSS) structure has been fabricated for use in a thermophotovoltaic system. The FSS provides a means for reflecting the unusable light below the bandgap of the thermophotovoltaic cell while transmitting the usable light above the bandgap. This behavior is relatively independent of the light's incident angle. The fabrication of the FSS was done using optical lithography and a phase-shift mask. The FSS cell consisted of circular slits spaced by 1100 nm. The diameters and widths of the circular slits were 870 nm and 120 nm, respectively. The FSS was predicted to pass wavelengths near 7 μm and reflect wavelengths outside of this pass-band. The FSSs fabricated performed as expected with a pass-band centered near 5 μm.

I. Introduction

Frequency selective surfaces (FSS) provide a method for constructing a mirror whose reflection and transmission properties vary with wavelength but are relately insensitive to the angle of incidence. FSSs have been used in radome design at microwave wavelengths[1,2] as well as for various optical elements at far infrared wavelengths[3,4]. Advances in microfabrication have allowed the fabrication of FSSs which operate at infrared and near infrared wavelengths. To fabricate features with the critical dimensions necessary for response in the infrared, methods

* Electronic mail: spector@ll.mit.edu

such as masked electron beam lithography[5], ion beam lithography[6], and nanoimprint lithography[5] have been employed. In this work, the fabrication of an infrared FSS was achieved using optical lithography. Compared to the other fabrication methods, optical lithography offers the advantage of being an established manufacturing technique which can achieve high throughput, good uniformity, and repeatability.

The FSS described here is a demonstration of a type of a wavelength selective filter which can be used to increase the efficiency of a thermophotovoltaic (TPV) system. In such a system, electricity is produced by converting infrared radiation from a heat source into electricity using a compound semiconductor thermophotovoltaic cell. Such a cell can only convert light with a wavelength shorter than the bandgap (λ_g) of the cell. The bandgap wavelength of the TPV system considered in this paper is ~2.5 μm. To improve the efficiency of the system, a FSS is placed between the heat source and the TPV cell. The FSS reflects light with a wavelength longer than the bandgap back to the heat source rather than wasting this energy. Because the TPV cell is most efficient for wavelengths just shorter than the bandgap wavelength, it is desirable to have such light transmitted by the FSS with a minimum amount of absorption and reflection. Because the light from the heat source may strike the FSS at various angles, the FSS performance also needs to be independent of the angle of incidence.

II. Fabrication

The design for the FSS contains a hexagonal array of circular slits or rings spaced by 1100 nm center to center. The diameter and the linewidths of the circular slits are nominally 900 and 100

nm, respectively. Another common geometry used in FSSs is the cross-dipole structure[5,6]. However, the ring structure is believed to be a better choice for TPV applications because the ring geometry is less sensitive to polarization and the angle of incidence[7]. The resonant wavelength of a free standing ring structure can be estimated as being equal to the ring's circumference[8]. When placed on a substrate, however, the resonant wavelength is shifted by an effective refractive index which is a combination of the indices of the substrate and the air above the FSS, giving the expression:

$$\lambda_{res} = C\left[\left(n_1^2 + n_2^2\right)/2\right]^{1/2}, \qquad (1)$$

where λ_{res} is the resonant wavelength, n_1 and n_2 are the refractive indices of the air above the FSS and of the substrate, and C is the circumference of the ring structures. Using Eq. 1, the estimated resonant wavelength of the ring structures described above is 7 μm. Because the FSS design contains circular slits cut into an otherwise reflective metal film, the resonant behavior of the FSS primarily allows transmission of light that is near the resonant. Light which is not near resonance is reflected.

The fabrication of the FSS was done using deep UV lithography and a chromeless phase-shift mask. The use of phase-shift masks in optical lithography is a resolution enhancement technique which has demonstrated feature sizes as small as 50 nm[9]. In this technique a chromeless mask with an etched 180° phase step is used. When projected, the phases from each side of the step destructively interfere producing a narrow dark line. The width of this line is given by the formula:

$$w_{FWHM} = \frac{0.25\lambda}{NA}, \qquad (2)$$

where w_{FWHM} is the width of the dark line (full width at half maximum) and NA is the numerical aperture of the projection system. Although phase-shift masks have the ability to create narrow lines, this simple chromeless mask technique is constrained to only create lines that follow non-intersecting closed paths. The ring structures fabricated here do not violate this constraint and are ideally suited for fabrication with phase-shift masks.

To understand the limits of what features could be fabricated, aerial image simulations were done with PROLITH software[10] (a commercial package). Hexagonal mask structures were used in the simulations, with the flat sides of the hexagons facing each hexagon's neighbors. Fig. 1 shows the aerial image predicted by a simulation with a 900 nm wide hexagon in an 1100 nm pitch array. The parameters used in the simulation correspond to the parameters of the system used for fabrication: λ=248 nm, NA=0.6, σ=0.3, where σ is the partial coherence. Note that the hexagonal character of the mask is largely lost, and the figures look like rings. As expected the most difficult part of the pattern to resolve is the gap at the closest point between rings. Close inspection of the simulation result reveals that it should be possible to produce 100 nm gaps and ring widths (see the caption for Fig. 1) with exactly the right threshold. However, the contrast between the rings and the gap is somewhat low. It should be noted that the spacing between rings, 200 nm, is smaller than the limit of 207 nm implied by Eq. 2. The simulation also predicts that the width of the rings will vary between 89 and 100 nm. This can be thought of as an example of an optical proximity effect. The line widths of the rings are wider where they are closest to their neighbor.

Simulations were also done on masks with smaller hexagons with the same spacing. As expected, smaller hexagons were resolved with greater separation between rings. For example, an 875 nm wide hexagon is predicted to produce 122 nm gaps and 108 nm wide rings. The contrast in this example is also more than 1 1/2 times greater than the above case of 900 nm wide hexagons. To test printability of the different sized features, a mask was generated that contained arrays of hexagons with nominal widths of 870, 880, and 900 nm. Also created on the mask were arrays of circles with 870 and 900 nm diameters. All of the arrays contained features on an 1100 nm pitch.

The process for fabricating the FSSs consisted of a single lithography step followed by metallization and lift-off. First, UV5 photoresist (manufactured by Shipley) 465 nm thick was applied to silicon wafers. Standard process conditions for the photoresist were used, with one notable exception. Before post-exposure bake the sample was dipped in a weak base solution consisting of 1 part 0.26 M TMAH in 100 parts deionized water. This weak base creates a thin inhibition layer at the top surface of the photoresist. This inhibition layer develops to a slightly smaller feature size, creating a re-entrant or T-topped profile. The profile improves lift-off by preventing the coating of the sidewalls of the resist during metallization. Metallization was done by electron beam evaporating 80 or 100 nm of gold or aluminum. A 5 nm evaporation of Ti preceded the gold evaporation to improve adhesion. Lift-off was done using warm ACT1 stripper with ultrasonic agitation.

III. Results

Attempts were made at printing rings in resist using the five different types of patterns listed above. Fig. 2 shows a series of SEM images of resist summarizing results from these tests. Hexagons with widths of 880 and 900 nm could not produce rings which could be resolved. The 870 nm wide hexagons and 870 nm diameter circles both successfully produced resolved rings, but the circles produced rings of much higher quality. The 900 nm circles nearly produced resolved rings. The rings would just start to have breaks in them at a dose (time of uv light exposure) sufficient to produce the gap between the rings. In all but the 870 nm circle images, there is a hexagonal structure visible. This hexagonal structure does not correspond to the hexagons of the mask, but is actually rotated 30° from the angle of the hexagons in the masks. The cause of this hexagonal structure is the proximity effect mentioned above.

For further inspection, a sample with the pattern in resist was cross-sectioned and imaged. An SEM image of the cross-sectioned resist is shown in Fig. 3. This image represents results from the 870 nm (diameter) circle region of the mask. Visible in the resist (cylinders) are bands caused by the standing waves (variations in cylinder diameter with height) . Because no antireflection coating was used, the reflection from the silicon substrate caused the strong standing waves, which resulted in these bands. Also visible in the cylindrical features is the desired T-topping. Although the T-topping is subtle, with only about 10 nm of overhang, this is sufficient to provide good lift-off. (A much larger overhang is undesirable and would result in a loss of resolution of the process). The cylindrical structures in Fig. 3 appear to be cone shaped; the rings appear narrower at the top than at the bottom. This shape is believed to be an artifact of

the SEM imaging process. If this were the true shape of the resist, it is unlikely that the lift-off procedure would have been so successful.

Fig. 4 shows the final FSS after metallization and lift-off. In this picture the FSS is constructed of an 80 nm thick gold layer. Similar results were obtained with aluminum and gold films 100 nm thick. The measured performance of a gold FSS, 100 nm thick is shown in Fig. 5. In the figure the transmission at normal incidence is plotted along with the reflection at near normal incidence (11°). The FSS is reflective at longer wavelengths and becomes transmissive near a wavelength of 5 μm. At wavelengths much shorter than 5 μm the FSS is primarily reflective again. Thus the FSS performs as expected, except that the resonant wavelength is shifted slightly from the estimated wavelength of 7 μm.

The reflectance of FSSs constructed of gold and aluminum were measured and compared. Fig. 6 shows the comparison between FSSs constructed of gold and aluminum. This time the reflectance was measured at an incident angle of 45°. There is little difference between the aluminum and gold FSSs, demonstrating that both materials are suitable for use at these wavelengths. Also, the measured reflectance at near normal incidence and at 45° both show a minimum at 5 μm demonstrating the desired insensitivity to the incident angle. The reflectance of a similar bare silicon substrate is also plotted on the same graph. The silicon substrate is not ideal for this (TPV) application because it's reflectance is nearly 50% at the low cell band gap wavelength of 2.5 microns. It is likely that the use of silicon is limiting the reflectance dip (and transmission peak) to only reach near 50%.

Because the TPV cell in this application has a band gap wavelength of 2.5 μm, the final FSS will require a resonant wavelength less than 2.5 μm. The FSS fabricated here demonstrated frequency selective functionality, but the FSSs design will need to be altered to achieve a shorter resonant wavelength. To achieve a shorter resonant wavelength, the FSS can be made of smaller ring structures and/or be built on a lower index substrate. Simulations performed indicated that it should be possible to build ring structures with diameters as small as 300 nm on 500 nm pitch using the same optical system parameters. It should also be possible to construct the FSS on a SiO_2 film, changing the substrate's index from 3.4 to 1.5. Together, these changes should allow the FSS's resonant wavelength to be shifted to achieve a shorter resonant wavelength.

The performance of the FSS can be further enhanced by the use of multiple FSS layers[11,12]. The use of aluminum as the metal for the FSS should allow the fabrication of multiple aluminum and SiO_2 layers using slightly modified standard microelectronic fabrication processes. Previously it was demonstrated that aluminum performs nearly identically to gold at wavelengths > 1 μm, making it a suitable choice for this application.

IV. Conclusion

Frequency selective surfaces (FSS) with an infrared resonant wavelength have been fabricated using deep UV optical lithography and phase-shift masks. The design for the FSS contained a hexagonal array of tightly packed circular slots (ring apertures). The circular slots were spaced by 1100 nm, and had inner and outer diameters of 870 nm and 1200 nm. Such a structure was predicted to have a resonant wavelength near 7 μm. FSSs were fabricated using one of two metals, gold and aluminum. Although there was a small shift in resonant wavelength to about 5

μm, both materials performed similarly and as expected. Although the TPV application requires a resonant wavelength shorter than demonstrated, there is a straightforward path to achieving a shorter resonant wavelength. Smaller ring structures and the use of a lower index substrate can provide the necessary shift of the resonant wavelength. FSSs with the desired properties for this TPV application should be manufacturable using these methods.

Acknowledgements:

The authors gratefully acknowledge the assistance of S. Deneault, M. Fritze, K. Krohn, and D. M. Lennon. This work was sponsored by the Department of Energy under Air Force Contract No. F19628-00-C-0002. The opinions, interpretations, conclusions, and recommendations are those of the authors and are not necessarily endorsed by the United States Air Force.

References:

[1]E. L. Pelton and B. A. Munk, IEEE Trans. Antennas Propag., **AP-22**, 800 (1974).

[2]S. W. Lee, IEEE Trans. Antennas Propag., **AP-19**, 656 (1971).

[3]R. Ulrich, K. F. Renk, and L. Genzel, IEEE Trans. Microwave Theory Tech., **MTT-11**, 363 (1963).

[4]R. Ulrich, Appl. Opt., **7**, 1987 (1968).

[5]Irina Puscasu, G. Boreman, R. C. Tiberia, D. Spencer, and R. R. Krchnavek, J. Vac. Sci. Technol. B **18**, 3578 (2000).

[6]M. D. Morgan, W. E. Horne, V. Sundaram, J. C. Wolfe, S. V. Pendharkar, and R. Tiberio, J. Vac. Sci. Technol. B **14**, 3903 (1996).

[7]T. K. Wu, Microwave and Opt. Technol. Let., **15**, 9 (1997).

[8]T. K. Wu, *Frequency Selective Surface and Grid Array*, (Wiley, New York, 1995), pp.2-9.

[9]M. Fritze *et al.*, J. Vac. Sci. Technol. B **18**, 2886 (2000).

[10]C. A. Mack, Proc. SPIE **538**, 207 (1985).

[11]B. A. Munk, R. J. Luebbers, and R. D. Fulton, IEEE Trans. Antennas Propag, **AP-22**, 804 (1974).

[12]B. A. Munk, *Frequency Selective Surfaces*, (Wiley, New York, 2000).

Figure Captions:

Fig. 1. Contour plot of simulated aerial image of 900 nm wide hexagon in a 1100 nm pitch array. Although contrast is low, this image predicts that the resolution of rings with 100 nm gaps and 100 nm ring widths may be possible.

Fig. 2. Experiment demonstration of the printability of mask features. The top row contains examples of printing from the hexagon features on the mask with widths of 870, 880, and 900 nm. The bottom row contains examples of printing from the circular features on the mask with diameters of 870 and 900 nm.

Fig. 3. Scanning electron microscope (SEM) image of the ring structures fabricated in resist. Visible are the desired small amounts of T-topping and standing waves. The cone-like shape of the rings is believed to be an artifact caused by the SEM exposure of the resist

Fig. 4. SEM image of a frequency selective surface (FSS) fabricated in gold, 80 nm thick.

Fig. 5. Performance of gold FSS at normal and near normal incidence. The FSS shows a band of transmission at 5 μm and reflection at other wavelengths.

Fig. 6. Reflectance of a gold FSS, aluminum FSS, and silicon wafer at 45° angle of incidence. Similar performance is shown for both materials (gold and aluminum). Also, the performance near normal incidence (Fig. 5) is similar for both materials.

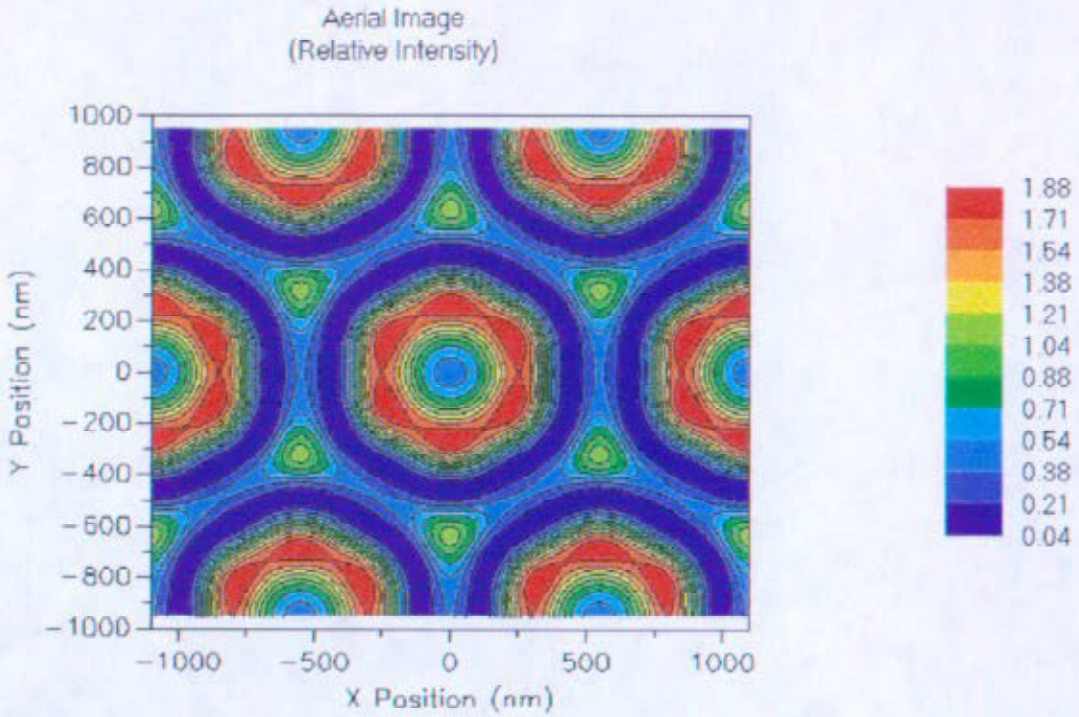
Aerial Image
(Relative Intensity)
Y Position (nm)
1000
800
600
400
200
0
-200
-400
-600
-800
-1000
-1000
-500
0
500
1000
X Position (nm)
1.88
1.71
1.54
1.38
1.21
1.04
0.88
0.71
0.54
0.38
0.21
0.04

Figure 1.

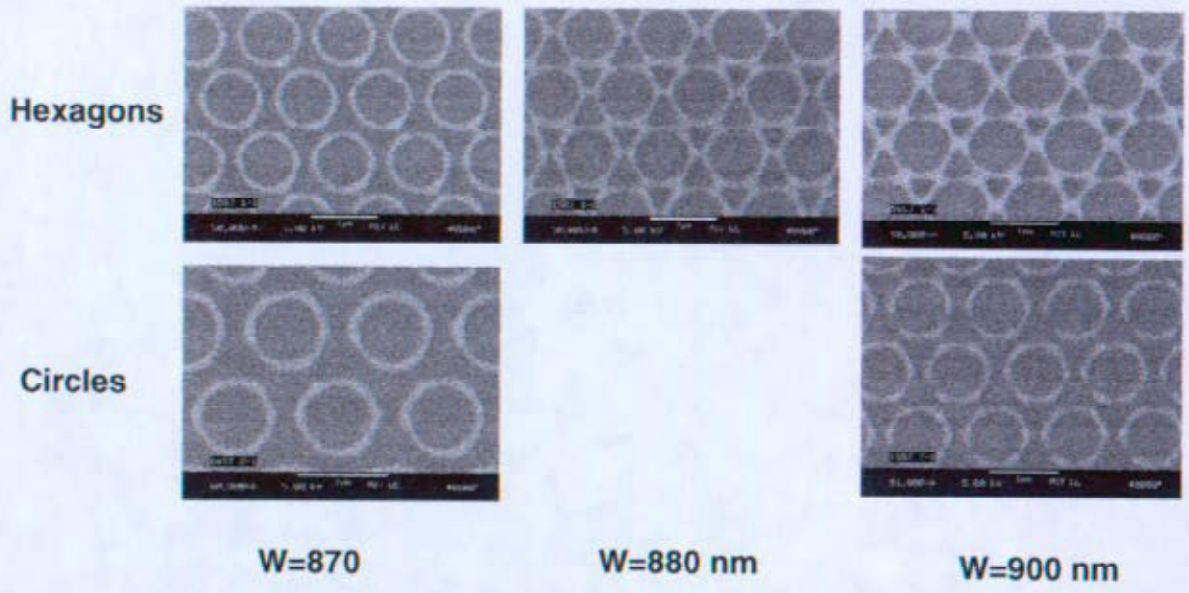

Figure 2.

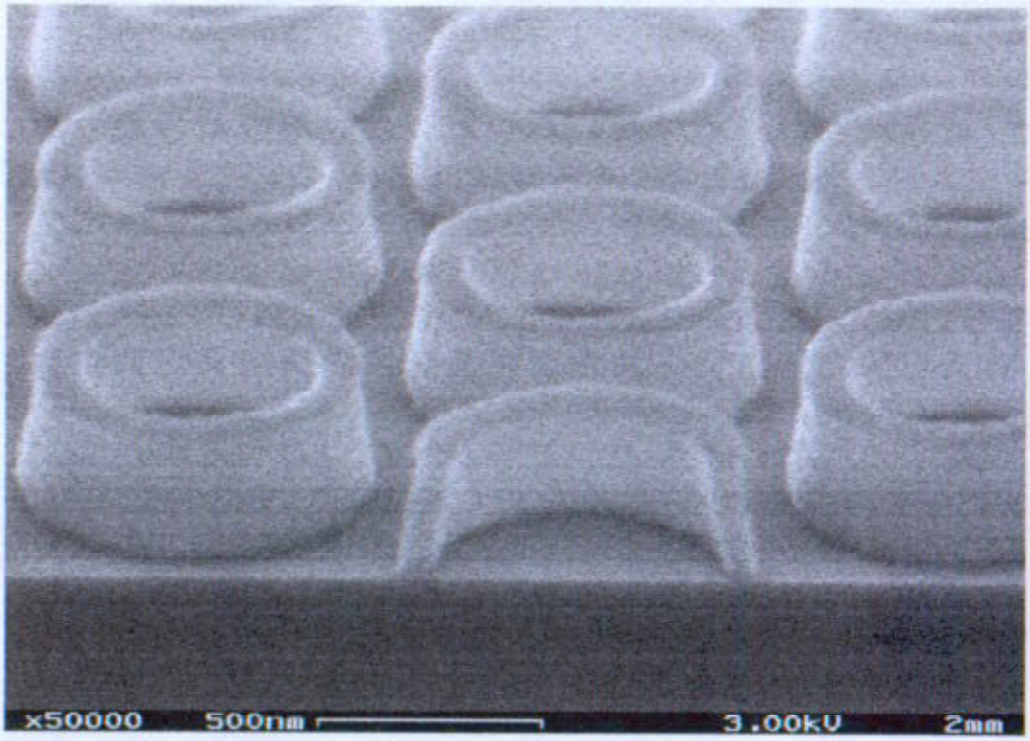

Figure 3.

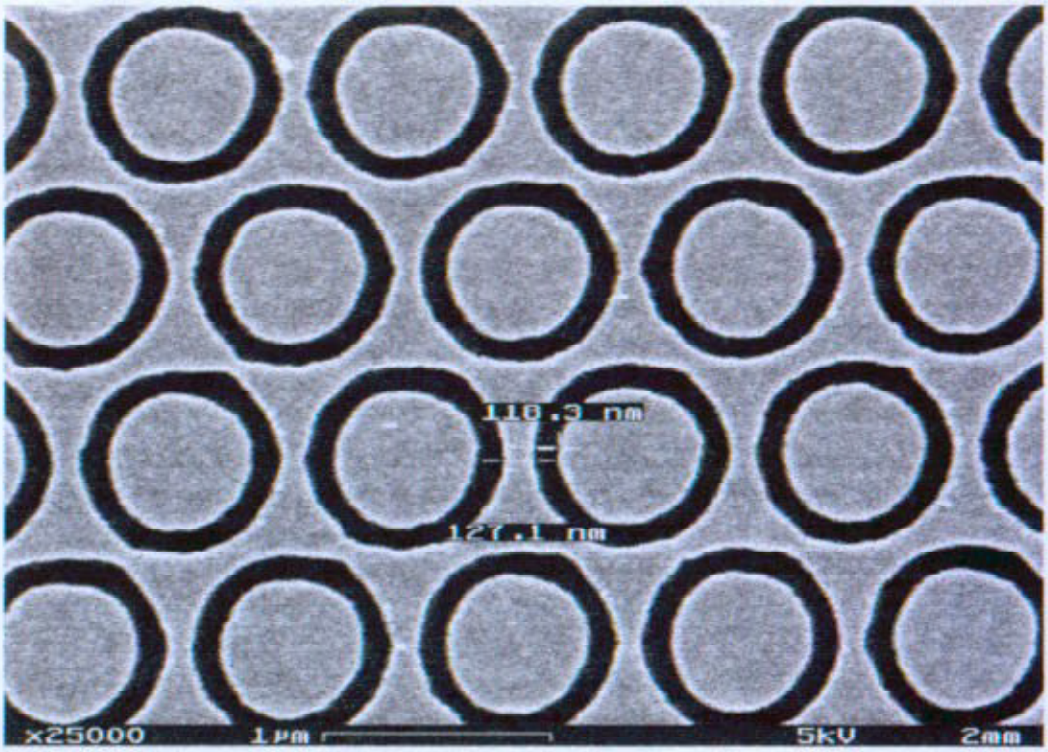

Figure 4.

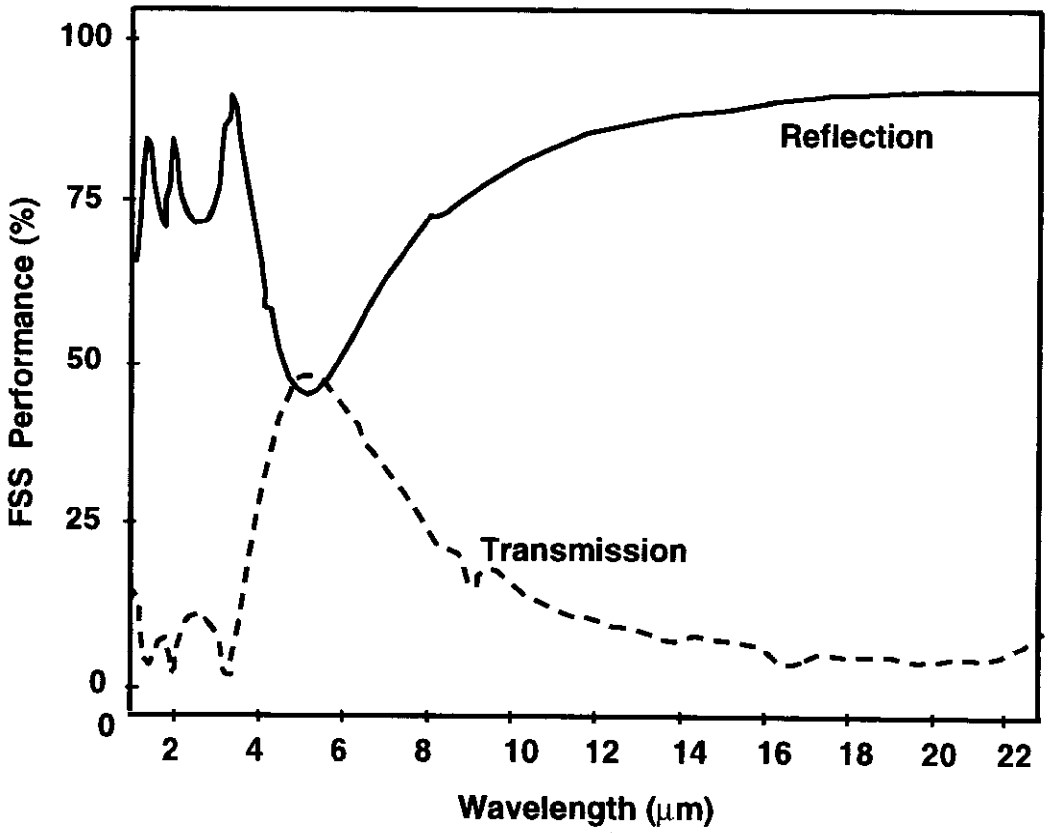
100
75
50
25
0
0
2
4
6
8
10
12
14
16
18
20
22
FSS Performance (%)
Wavelength (μm)
Reflection
Transmission

Figure 5.

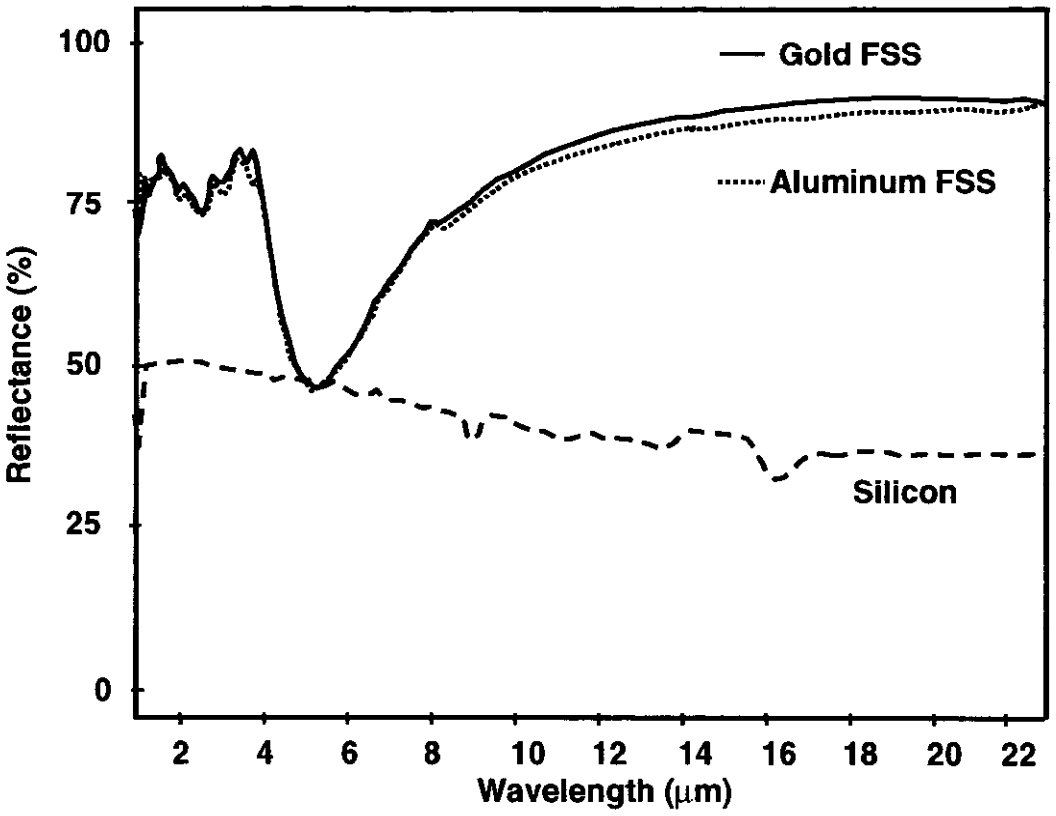
100
75
50
25
0
Reflectance (%)
2
4
6
8
10
12
14
16
18
20
22
Wavelength (μm)
Gold FSS
Aluminum FSS
Silicon

Figure 6.